Icarus 226 (2013) 419–427

Contents lists available at SciVerse ScienceDirect

Icarus

journal homepage: www.elsevier.com/locate/icarus

Evidence of a metal-rich surface for the Asteroid (16) Psyche from interferometric observations in the thermal infrared ☆

Alexis Matter [a,*], Marco Delbo [b], Benoit Carry [c], Sebastiano Ligori [d]

[a] Max Planck institut für Radioastronomie, auf dem Hügel, 69, 53121 Bonn, Germany
[b] UNS-CNRS-Observatoire de la Côte d'Azur, Laboratoire Lagrange, BP 4229 06304 Nice cedex 04, France
[c] IMCCE, Observatoire de Paris, UPMC, CNRS, 77 Av. Denfert Rochereau, 75014 Paris, France
[d] INAF-Osservatorio Astronomico di Torino, Strada Osservatorio 20, Torino, 10025 Pino Torinese, Italy

ARTICLE INFO

Article history:
Received 6 January 2013
Revised 10 June 2013
Accepted 10 June 2013
Available online 19 June 2013

Keywords:
Asteroids
Asteroids, Surfaces
Infrared observations
Data reduction techniques

ABSTRACT

We describe the first determination of thermal properties and size of the M-type Asteroid (16) Psyche from interferometric observations obtained with the Mid-Infrared Interferometric Instrument (MIDI) of the Very Large Telescope Interferometer. We used a thermophysical model to interpret our interferometric data. Our analysis shows that Psyche has a low macroscopic surface roughness. Using a convex 3-D shape model obtained by Kaasalainen et al. (Kaasalainen, M., Torppa, J., Piironen, J. [2002]. Icarus 159, 369–395), we derived a volume-equivalent diameter for (16) Psyche of 247 ± 25 km or 238 ± 24 km, depending on the possible values of surface roughness. Our corresponding thermal inertia estimates are 133 or 114 J m^{-2} s$^{-0.5}$ K^{-1}, with a total uncertainty estimated at 40 J m^{-2} s$^{-0.5}$ K^{-1}. They are among the highest thermal inertia values ever measured for an asteroid of this size. We consider this as a new evidence of a metal-rich surface for the Asteroid (16) Psyche.

1. Introduction

Asteroids classified in the X-complex (in the taxonomies by Bus and Binzel (2002) and DeMeo et al. (2009)) are characterized by a visible and near-infrared reflectance spectrum that is essentially featureless and moderately red in the [0.3–2.5] μm region. The spectroscopic X-complex can be split into three taxonomic classes, E, M and P, according to albedo (Tholen, 1984). M-type asteroids are distinguished by exhibiting moderate geometric visible albedos of about 0.1–0.3. Due to the lack of absorption features in the spectrum of M-type asteroids, the nature of these objects remains uncertain. Historically, M-class asteroids were assumed to be the exposed metallic core of differentiated parent bodies that were catastrophically disrupted, and thus the source of iron meteorites (Bell et al., 1989; Cloutis et al., 1990). While the parent bodies of meteorites are usually assumed to have formed in the main belt, Bottke et al. (2006) showed that the iron-meteorite parent bodies most probably formed in the terrestrial planet region. Some of the metallic objects currently located in the main-belt may thus not be indigenous but rather remnants of the precursor material that formed the terrestrial planets including the Earth. Therefore, those objects play a fundamental role in the investigations of the Solar System formation theories. Radar observations provided strong evidences for the metallic composition of a least some M-type asteroids. Very high radar albedos have been measured for various asteroids of this class, consistent with high concentration of metal (Ostro et al., 1985; Shepard et al., 2008). Moreover, the average density of two multiple M-type asteroids, 3.35 g cm^{-3} (Descamps et al., 2008) for (22) Kalliope and 3.6 g cm^{-3} (Descamps et al., 2011) for (216) Kleopatra, appeared to be significantly larger than the density of C-type or S-type asteroids (Carry, 2012). This is a strong evidence of difference in internal composition between M and C-type asteroids. However, recent visible and near-infrared spectroscopic surveys on about 20 M-type asteroids, including those exhibiting high radar albedos, detected subtle spectral absorption features on most of them (Hardersen et al., 2005; Fornasier et al., 2010). The most common one being the 0.9 μm absorption feature, attributed to orthopyroxene, and thus indicating the presence of silicate on their surface. From a survey of the 3 μm spectrum of about 30 M-type asteroids, Rivkin et al. (1995, 2000) also found hydration features on a tens of them. On the basis of these observations, they suggested that the original "M" class should be divided into "M" asteroids that lack hydration features such as (16) Psyche and (216) Kleopatra, and "W" asteroids that are hydrated such as (21) Lutetia. All of that confirms that most of the objects defined by the Tholen M-class have not a pure

☆ Based on observations collected at the European Southern Observatory (ESO), Chile: ESO Program ID 386.C-0928.

* Corresponding author. Present address: Institut de planétologie et d'astrophysique de Grenoble, 414, rue de la Piscine, 38400 Saint Martin d'Hères, France. Tel.: +33 4 76 63 58 30, fax: +33 4 76 44 88 21.

E-mail addresses: alexis.matter@obs.ujf-grenoble.fr (A. Matter), delbo@oca.eu (M. Delbo), bcarry@imcce.fr (B. Carry), ligori@oato.inaf.it (S. Ligori).

0019-1035/$ - see front matter © 2013 Elsevier Inc. All rights reserved.
http://dx.doi.org/10.1016/j.icarus.2013.06.004

metallic surface composition but contain other species including silicate minerals. Therefore, better compositional constraints for the spectrally featureless bodies like M-type asteroids are essential in order to understand and constrain the thermal, collisional, and migration history of Main-Belt Asteroids (MBAs). This includes the detection of additional absorption features in their reflectance spectra and the determination of their surface properties including surface roughness and in particular thermal inertia.

Thermal inertia (Γ) is a measure of the resistance of a material to temperature change. It is defined by $\Gamma = \sqrt{\rho\kappa c}$, where κ is the thermal conductivity, ρ the material density and c the specific heat. The value of thermal inertia thus depends on the material properties (see Mueller, 2007 and references therein for a table of the thermal inertia value of some typical materials). On one hand, it primarily informs us about the nature of the surface regolith: a soil with a very low value of Γ, for instance in the range between 20 and 50 J m^{-2} s$^{-0.5}$ K^{-1}, is covered with fine dust like on Ceres (Mueller and Lagerros, 1998); an intermediate value (150–700 J m^{-2} s$^{-0.5}$ K^{-1}) indicates a coarser, mm- to cm-sized, regolith as observed on (433) Eros (Veverka et al., 2001a; Veverka et al., 2001b) and (25143) Itokawa (Yano et al., 2006), respectively; solid rock with very little porosity is known to have thermal inertia values of more than 2500 J m^{-2} s$^{-0.5}$ K^{-1} (Jakosky, 1986). On the other hand, thermal inertia can represent a proxy for the surface composition, especially due to its dependency on thermal conductivity and specific heat. This is particularly important in the context of the M-type asteroids study since metal is an excellent thermal conductor, potentially leading to an enhanced thermal inertia. The study of Opeil et al. (2010) showed that thermal conductivity is significantly higher for iron meteorites than for non-metallic ones. This motivates our work of determining thermal inertia on M-type asteroids such as (16) Psyche to assess the change in thermal inertia for asteroids of different composition but having a similar size, knowing that the presence and thickness of the surface regolith is generally assumed to depend on the asteroid's size (see, e.g., Bottke et al., 2005).

The Asteroid (16) Psyche is the largest known M-type asteroid, with an IRAS diameter of 253 ± 4 km (Tedesco et al., 2002). Nevertheless, many size estimates have been reported during the last decade. Cellino et al. (2003) derived an area equivalent diameter of 288 ± 43 km based on speckle interferometry; Lupishko (2006) derived a diameter of 213 km based on considerations on its polarimetric albedo; from adaptive-optics imaging, Drummond et al. (2008) derived a volume equivalent diameter of 262 ± 6 km; Shepard et al. (2008) derived a volume equivalent diameter of 186 ± 30 km based on radar imaging; from the analysis of medium infrared data from the AKARI satellite by means of the Standard Thermal Model (Lebofsky et al., 1986), Usui et al. (2011) derived a diameter of 207 ± 3 km; finally, Durech et al. (2011) derived a volume equivalent diameter of 211 ± 21 km by combining a shape model derived by lightcurve inversion with occultation observations of (16) Psyche. In any case, Psyche appears to be significantly larger than the 30–90 km diameter expected for the metallic core of a differentiated asteroid (Rivkin et al., 2000), questioning a purely metallic nature for this asteroid. All those size measurements led to significant differences between the average bulk density estimations reported in the literature. They range from 1.8 ± 0.6 g cm^{-3} (Viateau, 2000) to 3.3 ± 0.7 g cm^{-3} (Drummond and Christou, 2006) and even 6.58 ± 0.58 g cm^{-3} (Kuzmanoski and Kovačević, 2002), value which is more in agreement with a metallic composition and a very low macroporosity. Nevertheless, by combining all the independent size and mass estimates, an average density of 3.36 ± 1.16 g cm^{-3} was found (Carry, 2012). This is comparable to the density estimates reported for other M-type asteroids like (22) Kalliope (Descamps et al., 2008) and (216) Kleopatra (Descamps et al., 2011). In addition, (Shepard et al., 2010) measured a high radar albedo of 0.42, which is indicative of a metal-rich surface. However, the detection of a 0.9 μm absorption feature suggested the presence of silicates on its surface (Hardersen et al., 2005). In this context, Hardersen et al. (2005) and Shepard et al. (2010) suggested that (16) Psyche may be a collisional aggregate of several objects, including partial or intact metallic cores that have retained a portion of their silicate-rich mantle.

To put tighter constrains on the nature of (16) Psyche, we used mid-infrared interferometry to determine the thermal properties of this asteroid, and refine its size measurements. Interferometry basically provides direct measurements of the angular extension of the asteroid along different directions (Delbo et al., 2009). Interferometric observations of asteroids in the thermal infrared, where the measured flux is dominated by the body's thermal emission, are sensitive to the surface temperature spatial distribution in different directions on the plane of the sky. The typical spatial resolution is about 0.06″ in the case of our Psyche observations. As the surface temperature distribution of atmosphereless bodies is affected by thermal inertia and surface roughness, interferometric thermal infrared data can be used to constrain these parameters. In particular, thermal infrared interferometry can help to remove the degeneracy existing between the effect of the thermal inertia and surface roughness in one single epoch (see Figs. 7 and 8 in Matter et al. (2011)), providing that we have several interferometric measurements with different projected baseline lengths and orientations, during the asteroid rotation. Thermal properties (thermal inertia and surface roughness) can thus be better constrained by thermal infrared interferometry in combination with the classical disk-integrated radiometry. In this context, we obtained interferometric data on (16) Psyche using the MIDI instrument combining two of the Auxiliary Telescopes (ATs) of the VLTI. As in Matter et al. (2011), a thermophysical model (TPM), taking into account the asteroid's orbit, spin, shape, and heat diffusion into the subsurface, was used for the analysis of the whole data set.

In Section 2 we report the observations and the data reduction process that we adopted; in Section 3 we briefly remind the principles of the thermophysical model used for the interpretation of MIDI data, and we detail the shape models that we used; in Section 4, we present our results, followed by a discussion in Section 5.

2. Observations and data reduction

2.1. Observations

The observations of (16) Psyche were carried out in visitor mode, on 2010 December 30. Two ATs were used in the E0–G0 configuration (baseline B = 16 m). Sky quality was relatively good and stable during those nights (see Table 1). We adopted the typical observing sequence of MIDI, which is extensively described by Leinert et al. (2004). For each of the five observing epochs of (16) Psyche (indicated in Table 1), we obtained one measurement of the total flux and of the interferometric visibility, both dispersed over the N-band, from 8 to 13 μm. We used the HIGH-SENS mode, where the total flux of the source is measured right after the fringe tracking and not simultaneously. To disperse the fringes, we used the prism of MIDI, which gives a spectral resolution of $\frac{\lambda}{\Delta\lambda} \approx 30$ at λ = 10 μm. Our observations also included a mid-infrared photometric and interferometric calibrator HD 29139, taken from the ESO database using the Calvin tool,[1] which is the calibrator selector for the VLTI instruments (MIDI and AMBER). We remind that interferometric calibrators are stars that have small and known angular diameter, so that their visibility is close to unity at all wavelengths. This calibrator was chosen to have a minimum angular separation

[1] Available at http://www.eso.org/observing/etc/.

Table 1
Log of the observations for (16) Psyche and its calibrator HD 29139, both observed with two ATs in E0–G0 configuration. PBL and PBLA stand for Projected BaseLine, and Projected BaseLine Angle, respectively. The last column gives a label for each interferometric observation of (16) Psyche, the label 'Calib' indicating a calibrator observation.

Object	Date (UT)	PBL (m)	PBLA (°)	seeing (″)	Airmass	Label
HD 29139	2010–12–30 00:24	11.3	82.0	1.50	1.70	Calib
(16) Psyche	2010–12–30 00:48	11.88	82.7	1.15	1.60	1
HD 29139	2010–12–30 02:59	14.4	79.0	1.00	1.40	Calib
(16) Psyche	2010–12–30 03:18	15.8	74.1	0.70	1.37	2
(16) Psyche	2010–12–30 03:30	16.0	73.3	0.75	1.37	3
(16) Psyche	2010–12–30 03:40	16.0	72.6	0.70	1.39	4
HD 29139	2010–12–30 03:58	15.9	70.5	0.60	1.40	Calib
HD 29139	2010–12–30 04:33	15.6	67.5	0.64	1.50	Calib
(16) Psyche	2010–12–30 04:51	15.5	66.5	0.75	1.60	5

with the source (≈3°) and a similar airmass, as shown in Table 1. This Table also summarizes the log of observations, with the corresponding interferometric parameters.

2.2. Data reduction

Extraction and calibration of the flux and visibility measurements of (16) Psyche were performed using the data reduction software package EWS (Expert WorkStation). This publicly available[2] software performs a coherent analysis of dispersed fringes to estimate the complex visibility of the source. The method and the different processing steps are described in Jaffe (2004). The calibration of the fluxes and visibilities was performed using the closest calibrator observation in time. Calibrated fluxes of (16) Psyche were obtained by multiplying the ratio target/calibration star raw counts, measured by MIDI at each wavelength, by the absolute flux of the calibrator. The absolutely calibrated infrared spectrum of our calibrator was taken from a database created by R. van Boekel, which is initially base on infrared templates created by Cohen et al. (1999). More details can be found in Verhoelst (2005). The instrumental visibilities of (16) Psyche correspond to the ratio of the source raw correlated flux and the source raw photometric flux. The calibrated visibilities of (16) Psyche were then derived by dividing the instrumental visibility by the visibility measured on the calibrator for each observing epoch. We refer the reader to Delbo et al. (2009) for a more detailed description of the data reduction and calibration of MIDI interferometric data.

The five calibrated flux and visibility measurements of (16) Psyche are shown in Fig. 1. The error bars represent the statistical noise contribution affecting the correlated and total flux measurements. It is estimated by splitting a complete exposure, consisting of several thousand of frames, into five equal parts and deriving the variance of these sub-observations. In the error budget, we neglected the error due to the variability of the interferometer transfer function during the night. However this is not a problem since, by computing the rms of the transfer function, i.e., the instrumental visibility provided by the calibrator observations, we found a very good stability all over the night.

2.3. Observational results

At each observing epoch, the corresponding visibility is pretty low (≈0.1–0.4), thus indicating that the object is very well resolved by MIDI. Moreover we can notice a significant decrease of the visibility level between the first and second epochs, which are separated by 2h30, and then only slight changes in the visibility shape and level for the next epochs. This behavior can be explained by the increase of the length of the projected baseline during the observing night (see Table 1), combined to the evolution of the projected baseline orientation and the asteroid rotation. For instance, the difference between the first and last visibility measurements is mainly due to the increase of the projected baseline length since our observations covered a complete rotation of the asteroid (≈4.2 h), without a significant evolution of the baseline orientation. This is illustrated in Fig. 2, where we represented the expected orientation of (16) Psyche at the time of the VLTI observations. Here, we considered the two existing pole solutions derived by Kaasalainen et al. (2002) and that we detail hereafter in Section 3.

3. Thermophysical modeling

The thermophysical modeling of interferometric data is extensively described in Matter et al. (2011, and references therein), and here we briefly remind its principles, along with the shape model we used for this modeling.

The thermal inertia and macroscopic roughness of an asteroid can be derived by comparing measurements of the thermal-infrared flux and interferometric visibility of the body to synthetic fluxes and visibilities generated by means of a thermophysical model (TPM). A TPM uses the spin vector information to orient a 3-D shape model, composed of a mesh of planar facets, at the time of the observing epochs. The temperature of each facet is calculated by solving the one-dimensional heat diffusion equation (where the heat diffusion is between the surface and the shallow subsurface) using presets thermal inertia values. Surface roughness is modeled by adding hemispherical craters of variable opening angle, γ_c, and surface density, ρ_c. As for Delbo and Tanga (2009), thermal conduction within the craters is also modeled. Albedo, thermal inertia, surface roughness and emissivity are assumed constant over the asteroid's surface. We remind that emissivity, noted hereafter ϵ, has normally directional properties and drops at higher viewing angles, in particular at the limb of objects having a smooth surface (see e.g., Jakosky et al., 1990). However, we expect it to be a second-order effect since the limb normally contributes much less to the thermal emission than the nadir, especially if the object was observed under a low solar phase angle like for our observations of (16) Psyche. We also assumed ϵ achromatic and equal to 0.9, which is a typical value for silicate powders and is commonly assumed for the surface of asteroids (Emery et al., 2006; Mueller, 2007). However, regarding the possible metallic nature of the Psyche's regolith, it is worth mentioning that metals have usually emissivities lower than 0.9 depending on their state of roughness and porosity. For instance, powdered iron at a temperature of 300 K and with a porosity similar to the lunar regolith (≈50%), has $\epsilon \approx 0.8$ (Sih and Barlow, 2004). Assuming that the regolith of (16) Psyche is purely ferrous, we thus ran in parallel our TPM with $\epsilon = 0.8$. As a result, only tiny changes were observed in terms of size, thermal inertia and surface roughness. Moreover, silicate material was detected on the Psyche's surface (Hardersen et al., 2005), and could increase

[2] Software package is available at http://home.strw.leidenuniv.nl/j~affe/ews/index.html.

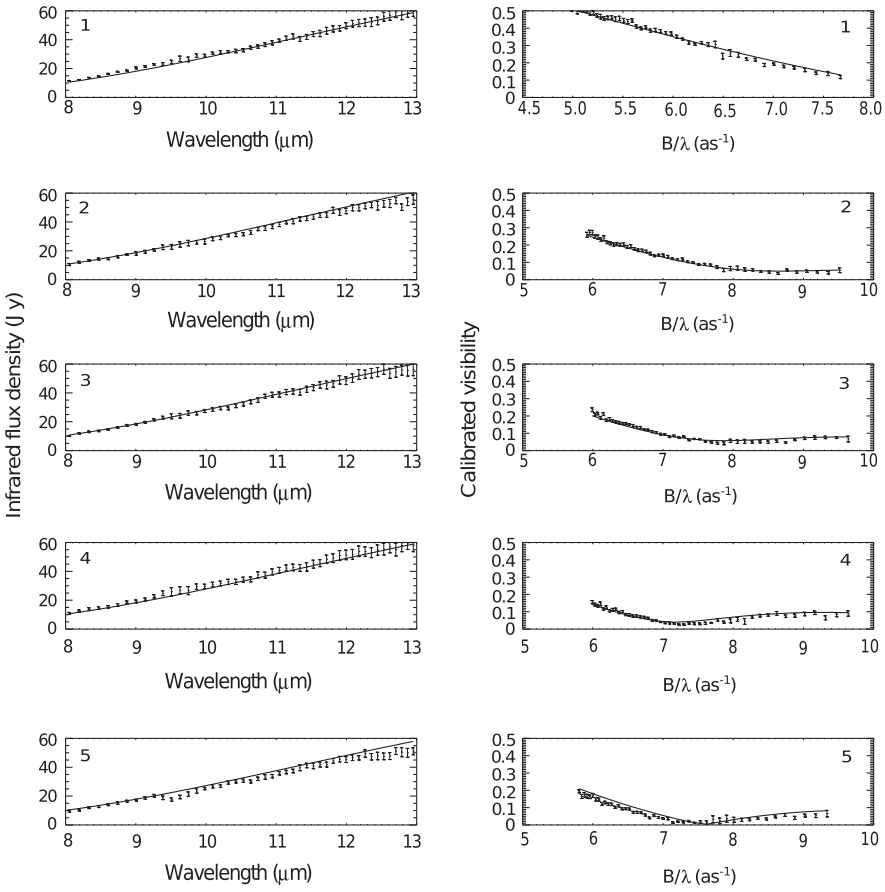

Fig. 1. *Left panels:* measured thermal infrared fluxes (with error bars) and best-fit TPM infrared fluxes (solid lines) of (16) Psyche, plotted between 8 and 13 μm. *Right panels:* measured mid-infrared interferometric visibilities (with error bars) and best-fit TPM visibilities (solid lines) of (16) Psyche, plotted as a function of angular frequency. The best-fit model represented here is: 'low roughness', $\Gamma = 115$ J m^{-2} s$^{-0.5}$ K^{-1}. For each pair of flux and visibility measurements, we indicated the label ('1', '2', '3', '4', '5') of the corresponding observing epoch, as defined in Table 1.

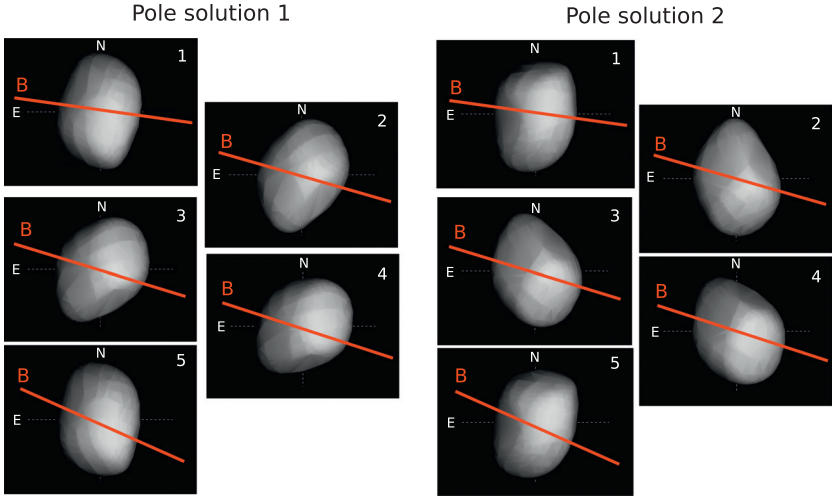

Fig. 2. Representation of the expected orientation of (16) Psyche along with the projected baseline orientation at the time of the VLTI observations, on the plane of the sky; the North (N) and East (E) directions are indicated. We used the convex mesh and the two existing pole solutions derived by Kaasalainen et al. (2002) and detailed in Section 3. For each epoch, we indicated the corresponding label (1–5), as defined in Table 1.

the surface emissivity. Therefore, we finally kept $\epsilon = 0.9$ for the thermophysical modeling of (16) Psyche.

Following the procedure described in Matter et al. (2011), the best-fit value of a, which is the linear mesh scale factor, for each discrete value of Γ and each roughness model can be found by minimizing a χ^2 function taking into account both the integrated flux and the interferometric visibility. Then, the location of the minimum χ^2 as a function of Γ gives the best-fit asteroid surface thermal inertia for each roughness model. Eventually, the value of a at Γ-minimum is used to determine the best-fit value of the

volume equivalent diameter of the mesh, $D_\vee = 2\left(\frac{3\vee}{4\pi}\right)^{\frac{1}{3}}$, where $\vee$ is the volume of the mesh.

Two convex mesh were downloaded from the Database of Asteroid Models from Inversion Techniques[3] (DAMIT, see Durech et al., 2010). Both shape models are characterized by a sidereal rotation period (P), and a pole solution giving the spin axis direction, which was initially derived by Kaasalainen et al. (2002) from inversion of optical lightcurves. Note that while inversion of optical lightcurves reconstruct the 3D shape of an asteroid, these shapes are convex by construction and do not provide any size information. The models derived from the optical lightcurves inversion are thus scaled to unity volume. Later on, the two shape models of (16) Psyche were refined and scaled by Durech et al. (2011) using occultation data. The associated two possible pole solutions are:

- solution 1: $\lambda_0 = 32°$ $\beta_0 = -7°$, $P = 4.195948$ h
- solution 2: $\lambda_0 = 213°$ $\beta_0 = 0°$, $P = 4.195948$ h

where λ_0 and β_0 are the ecliptic longitude and latitude of the spin axis direction (J2000.0, in degree), and P is the sidereal rotation period. The corresponding volume-equivalent diameters, derived from occultation data, are 211 ± 21 km (solution 1) and 209 ± 29 km (solution 2). Interestingly, Durech et al. (2011) reported that only the first pole solution reported by Kaasalainen et al. (2002) was consistent with all the occultation chords. Moreover, Hanus et al. (2012) identified the same best pole solution from comparison of adaptive-optics images and the shape models. They derived an equivalent diameter of 209 ± 9 km. In parallel, Kaasalainen et al. (2002) suggested the existence of albedo variegations over the surface of (16) Psyche. They detected the signature of a bright spot of moderate size, which is about 30% brighter than the rest of the surface. However, albedo variegations have little effect on the thermal emission. In particular, by increasing the geometric visible albedo of 30%, the 10 μm flux vary by about 2%, which is within the error bars of our MIDI measurements. Therefore, the assumption of thermal homogeneity (thermal inertia, surface roughness) over the asteroid surface should not be affected by this bright spot.

Using both shape models, the TPM was run for each roughness model, and thermal inertia values of 5, 10, 25, 50, 75, 100, 125, 150, 175, 200, 300, 400, 500, 750 and 1000 J m^{-2} s$^{-0.5}$ K^{-1}. The roughness models we used are: 'no roughness' ($\gamma_c = 0°$, $\rho_c = 0$), 'low roughness' ($\gamma_c = 45°$, $\rho_c = 0.5$), 'medium roughness' ($\gamma_c = 68°$, $\rho_c = 0.75$), and 'high roughness' ($\gamma_c = 90°$, $\rho_c = 1.0$). Then the fit procedure described in Section 3 was applied to the measured fluxes and visibilities, each of them containing 47 points between 8 and 13 μm. The flux and visibility measurements shown in Fig. 1 are the inputs of the thermophysical model.

In the next section we describe and discuss the results obtained from the application of the TPM to the observed visibilities and fluxes of (16) Psyche.

4. Results

Fig. 3 shows our reduced χ^2 estimator as a function of Γ for the four different roughness models, in the case of the two pole solutions described above.

We note that a surface with a low or no macroscopic roughness and a value of thermal inertia of about 130 J m^{-2} s$^{-0.5}$ K^{-1} give the best fit to the observations, for both pole solutions. However, it clearly appears that the pole and shape solution 1 gives a better fit to our MIDI data than the pole and shape solution 2, by a factor of about 5. This is in agreement with the conclusions of Durech et al. (2011) and Hanus et al. (2012) who favored the first pole solution. Therefore, we adopt the pole and shape solution 1 for the determination of thermal properties of (16) Psyche.

To refine the estimation of the best-fit thermal inertia values, we ran the TPM for additional values, namely, Γ = 105, 110, 115, 120, 130, 135, 140, 145, 155, 165. Then, using a polynomial interpolation, we found the minima of the 'no roughness' and 'low roughness' models at $\Gamma = 133$ and 114 J m^{-2} s$^{-0.5}$ K^{-1}, respectively. The reduced χ^2 values of those two best-fit models are 3.26 and 3.14, respectively. To obtain the best-fit values for $D_\vee$, we multiplied the volume-equivalent diameter of the mesh (211 km) by the best-fit scale factor values we got from our fit, namely 1.17 and 1.13 for the 'no roughness' and 'low roughness' models, respectively. The corresponding values of $D_\vee$ are 247 and 238 km, with associated p_V values of 0.12 and 0.13, respectively; for the calculation of p_V, we considered an absolute magnitude H of 5.93 according to Pravec et al. (2012).

In parallel, we also forced the volume equivalent diameter of the mesh to its nominal value (211 km for the solution 1) in order to assess its effect on our thermal inertia determination. We thus fixed the mesh scale factor to 1, and recalculated a χ^2 value for each roughness model and thermal inertia value. It appeared that the fit to the visibility and flux measurements is significantly worse for any roughness model ($\chi^2_{\text{red}} \geqslant 50$) while the best-fit values for thermal inertia are slightly lower (between 90 and 110 J m^{-2} s$^{-0.5}$ K^{-1}).

In Fig. 1 we plot the visibility and flux of the best-fit model ('low roughness', $\Gamma = 114$ J m^{-2} s$^{-0.5}$ K^{-1}, $D_\vee = 238$ km, $p_V = 0.13$), in addition to the measured fluxes and visibilities of (16) Psyche. We note that our model represents well the observed flux except for the long-wavelength edge of the N band. Indeed, for the second and fifth observing epochs, the TPM flux is greater than the measured one by roughly 10% at 13 μm. This 'offset-like' mismatch may come from an underestimation of the total flux of the source by MIDI, due to a bad estimation and subtraction of the thermal background (and its fluctuations), which is dominant in the mid-infrared (see, e.g., Perrin et al., 2003). This is especially problematic around 13 μm where the atmospheric transmission starts to be degraded by water absorption lines. Since the MIDI correlated flux measurements are usually not very much affected by background subtraction (see e.g., Chesneau, 2007), an underestimation of the photometry would bring an increase in the visibility. However, since the fringe contrast is low, this effect is not noticeable in our visibility measurements. The fit to the visibilities generally appears good and follow the same trend as the measurements, confirming the good match of the shape model to the interferometric data.

In order to search for the presence of possible emission features in the mid-infrared spectrum of (16) Psyche, we plotted in Fig. 4 the ratio between the MIDI flux measurement and our best-fit TPM for each observing epoch. Only the first epoch shows marginal detection of a possible emission feature between 8 and 10 μm that could be associated with the Christiansen peak around 9 μm. The error bars shown in Fig. 4 represent the statistical uncertainty affecting the MIDI measurements. However, bad estimation and removal of the strong thermal background over the N band and/or the atmospheric ozone absorption feature around 9.6 μm can imply additional uncertainties of the order of 10% on the absolute level of MIDI photometry measurements (see e.g., Chesneau, 2007). We thus think this most likely applies to the 'absorption feature' around 9.6 μm in the fifth epoch plot, and then probably also to the 'emission' pattern between 8 and 10 μm in the first epoch plot. As a consequence, we cannot report with confidence the detection of an emission feature in the mid-infrared spectrum of (16) Psyche.

To estimate the statistical uncertainty affecting the fit parameters Γ and $D_\vee$, we followed the Monte-Carlo procedure described in Matter et al. (2011): 200 normally distributed flux and visibility

[3] http://astro.troja.mff.cuni.cz/projects/asteroids3D/.

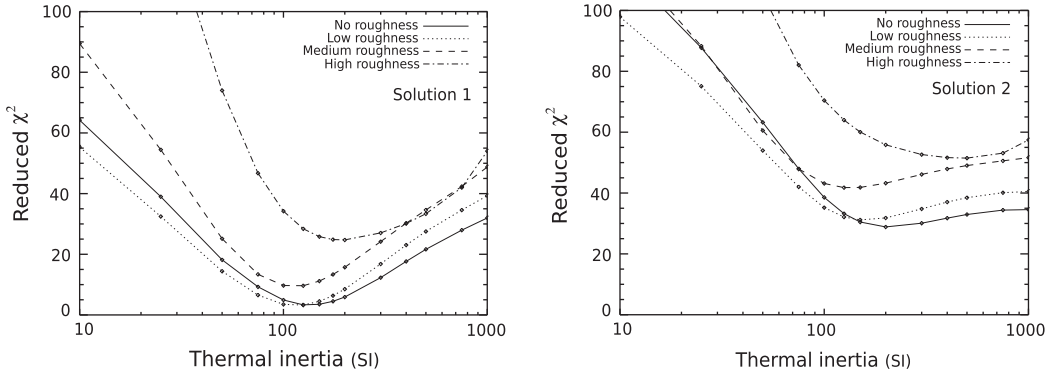

Fig. 3. *Left:* plot of the reduced χ^2, calculated from the TPM in the case of the first pole solution, as a function of thermal inertia Γ, for the four roughness models (see Section 3). *Right:* reduced χ^2, calculated from the TPM in the case of the second pole solution.

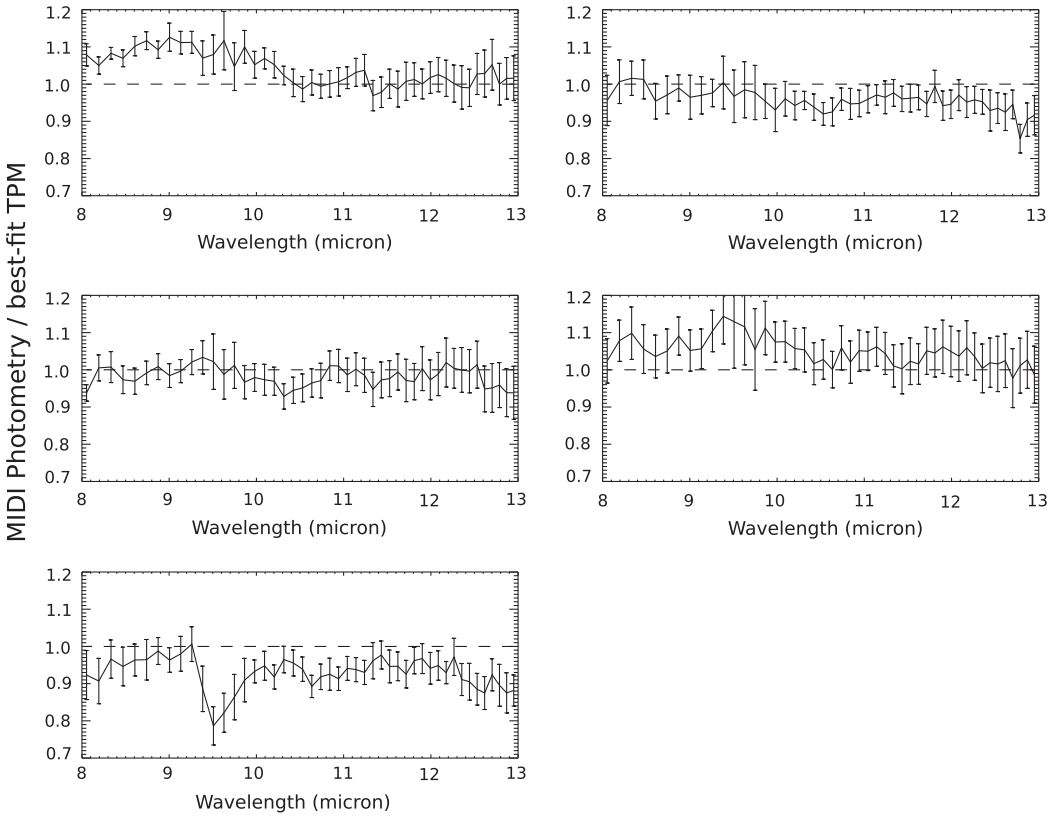

Fig. 4. Ratio of the MIDI flux over the best-fit TPM shown in Fig. 1, namely 'low roughness' and $\Gamma = 115\ \mathrm{J\,m^{-2}\,s^{-0.5}\,K^{-1}}$. We indicated the label corresponding to each observing epoch ('1'–'5'). Since we assumed an emissivity of 0.9 in our TPM, the level of the continuum (dashed line) is at 1.

values per observation were generated at each wavelength, with average and standard deviation matching the data within their respective 1-σ uncertainty; then for each set of fluxes and visibilities, a new χ^2 was computed; finally we took the standard deviation of the best-fit Γ and $D_\vee$ values, found for all the synthetic data sets, as the 1-σ uncertainty on our best-fit value for Γ and $D_\vee$. As a result we find $\Gamma = 133 \pm 2\ \mathrm{J\,m^{-2}\,s^{-0.5}\,K^{-1}}$, $D_\vee = 247 \pm 1$ km as the best fit solution for a model without roughness; and $\Gamma = 115 \pm 2\ \mathrm{J\,m^{-2}\,s^{-0.5}\,K^{-1}}$, $D_\vee = 238 \pm 1$ km as the best fit solution for a model with a low roughness. Therefore, the 1-σ statistical error from the Monte Carlo procedure is about 1% on the volume equivalent diameter and 2% on the thermal inertia. This is very low, as expected from the statistical noise affecting the MIDI measurements, and probably underestimates the true uncertainty on our thermal inertia and diameter estimates. Indeed, in thermophysical modeling, this uncertainty is generally dominated by the model systematics, as this was the case for the first thermophysical modeling of the interferometric data of (41) Daphne. Matter et al. (2011) estimated such a systematic error to be of about 7% on the diameter, taking into account only the contribution from the surface roughness modeling. In the case of (16) Psyche, the model systematics due to the surface roughness modeling is estimated by considering the two plausible solutions in terms of our best-fit indicator, i.e., no roughness and $\Gamma = 133\ \mathrm{J\,m^{-2}\,s^{-0.5}\,K^{-1}}$, and low roughness and $\Gamma = 114\ \mathrm{J\,m^{-2}\,s^{-0.5}\,K^{-1}}$. The corresponding uncertainty would thus be 9 km, i.e., 3% in relative uncertainty for $D_\vee$, and $19\ \mathrm{J\,m^{-2}\,s^{-0.5}\,K^{-1}}$, i.e., 15% in relative uncertainty for Γ. However, the systematic uncertainty budget probably includes additional contributions from the spin solution, the assumption of isotropic emissivity, the shape model itself and especially the

albedo variegations that impact the optical lightcurves inversion process. This last point may be important here since Kaasalainen et al. (2002) found evidences of a bright spot (about 30% brighter) on one side of the (16) Psyche's surface. However, we could not properly estimate the contribution of these sources of uncertainty in the TPM. Therefore, we finally adopted a conservative error value of 10% in $D_{\vee}$, as generally considered in other thermophysical models (see, e.g., Mueller et al., 2010; Marchis et al., 2012). For thermal inertia, we estimated a conservative uncertainty of 40 J m^{-2} s$^{-0.5}$ K^{-1}, based on the shape of the χ^2 curve around the minima of the 'no roughness' and 'low roughness' models (see Fig. 3). The uncertainty on the p_V values are derived using the 10% relative error on $D_{\vee}$. Table 2 summarizes our results.

5. Discussion

5.1. Size and albedo

The best-fit values of $D_{\vee}$ obtained from our TPM analysis of MIDI data, 247 ± 25 km and 238 ± 24 km, presents an offset of about 30 km with the nominal value (211 ± 21 km). Even though these values are in agreement within the error bars, our TPM results seem to favor a larger diameter for (16) Psyche. We remind that the condition of convexity, imposed by the lightcurve inversion technique (see Kaasalainen and Torppa, 2001), may introduce such a systematic bias on the size determination when large concavities are present on the asteroid surface. In this case, the volume-equivalent diameter obtained when using a convex shape will overestimate the 'true' volume and then the size of the asteroid. In our preceding analysis of (41) Daphne with MIDI (Matter et al., 2011), we faced a similar situation. The volume-equivalent diameter derived with a convex shape model was overestimated, and the use of a more detailed shape model, including concavities (Carry, 2009), solved this discrepancy. Although the diameter values of 247 km and 238 km we derived here are close to the average diameter of all reported estimates for Psyche (247 ± 19 km, see Carry, 2012), we expect the real value to be somehow smaller.

Using our TPM diameter estimation, we derived a geometric visible albedo value in the range between 0.12 and 0.13. As expected from the IRAS and AKARI size estimates, our estimate lies between the values derived from those surveys, namely 0.120 ± 0.004 and 0.18 ± 0.01, respectively. Those values are not identical within uncertainties. This discrepancy is probably due to the fact that we are comparing our volume equivalent diameter estimate with instantaneous area equivalent diameters measured at different epochs. Nevertheless, those albedo values are in good agreement with the M-type taxonomic type of (16) Psyche (by definition, M-types have an albedo between 0.075 and 0.30).

5.2. Thermal properties

As detailed in the introduction, infrared interferometry can spatially probe the asteroid surface temperature distribution in different directions at high angular resolution. Used in combination with infrared radiometry, it can help to remove the degeneracy existing in our constraints of thermal inertia and surface roughness and this at one single epoch, as already shown in Matter et al. (2011).

We obtained good constraints on the determination of macroscopic roughness of (16) Psyche. Both no- and low-roughness models appears equally good in terms of our best-fit estimator. We estimate that the corresponding mean surface slope, as defined by Hapke (1984), should be lower than 10° for (16) Psyche. A high macroscopic roughness is discarded. We remind that the roughness is at scales ranging from several centimeters to a fraction of the length of a facet, the latter being of the order of 10 km. Interestingly, radar data reported by Shepard et al. (2008) give a very low polarization ratio of 0.06 ± 0.02 for (16) Psyche, which indicates a smooth surface without significant radar-wavelength-scale surface roughness. Nevertheless, this agreement has to be considered with caution since the macroscopic surface roughness probed by infrared interferometry may be at a scale different than that constrained by radar observations. In addition, our TPM analysis indicates that (16) Psyche has a thermal inertia value lying between 114 ± 40 and 133 ± 40 J m^{-2} s$^{-0.5}$ K^{-1}. This is significantly larger than the thermal inertia values generally measured on main-belt asteroids larger than 100 km in diameter (see Fig. 5). Indeed, large main-belt asteroids such as (1) Ceres, (2) Pallas, (3) Juno, (4) Vesta, (21) Lutetia, (41) Daphne, (65) Cybele, or (532) Herculina present a very low thermal inertia, between 5 and 30 J m^{-2} s$^{-0.5}$ K^{-1} (Mueller and Lagerros, 1998; Müller and Blommaert, 2004; Lamy et al., 2010; Matter et al., 2011). Mueller et al. (2010) also measured a low thermal inertia of 20 ± 15 J m^{-2} s$^{-0.5}$ K^{-1} for the large binary Trojan (617) Patroclus. More recently, Marchis et al. (2012) also found thermal inertia potentially lower than 100 J m^{-2} s$^{-0.5}$ K^{-1} for 200 km-class main-belt asteroids, except for the M-type Asteroid (22) Kalliope, which could exhibit a higher value (Γ = 5 – 250 J m^{-2} s$^{-0.5}$ K^{-1}). One exception is the Asteroid (694) Ekard for which Delbo and Tanga (2009) determined a thermal inertia value around 100–140 J m^{-2} s$^{-0.5}$ K^{-1}. However, the TPM fit to the IRAS data for this asteroid was the worst among those studied in that work, indicating that the thermal inertia value for (694) Ekard might be less accurate compared to the other values derived for asteroids with sizes larger than 100 km. All those measurements imply that the surfaces of those large bodies are likely covered by a thick layer of fine-grained dust regolith. This is expected for such large bodies that can gravitationally retain on their surface loose material like thin dust

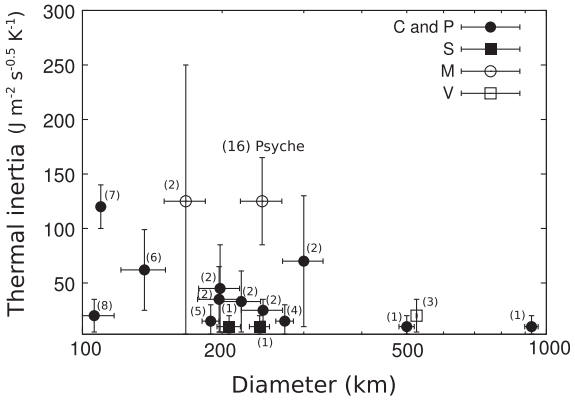

Fig. 5. Compilation of the existing thermal inertia measurements of main-belt asteroids larger than 100 km in diameter. We included our new measurement for (16) Psyche. We indicated the taxonomic type (C-complex, S-complex and V-type) of each asteroid following Bus and Binzel (2002), DeMeo et al. (2009). We separated the X-complex into M-type and P-type asteroids, following the Tholen classification, to emphasize the higher thermal inertia of M-type asteroids. We also mention the corresponding references for each measurement: (1) Mueller and Lagerros (1998), (2) Marchis et al. (2012), (3) Leyrat et al. (2012), (4) Müller and Blommaert (2004), (5) Matter et al. (2011), (6) Mueller et al. (2010), (7) Delbo and Tanga (2009), (8) O'Rourke et al. (2012).

Table 2
Results of the determination of physical properties of the Asteroid (16) Psyche, using the TPM. Γ is the thermal inertia, $D_{\vee}$ is the spherical volume equivalent diameter, and p_V is the geometric visible albedo. The errors represent an estimation of the dominant contribution of the model systematics, as explained in Section 4.

Roughness model	Reduced χ^2	Γ (J m^{-2} s$^{-0.5}$ K^{-1})	$D_{\vee}$ (km)	p_V
No roughness	3.3	133 ± 40	247 ± 25	0.12 ± 0.02
Low roughness	3.2	114 ± 40	238 ± 24	0.13 ± 0.03

produced from impact ejecta. On the other hand, smaller asteroids of a few km or tens of km in size have lower gravity and are expected to retain less regolith from impacts.

In general, existing measurements shows a decrease in the thermal inertia value with increasing asteroid diameter (see e.g., Delbo et al., 2007; Delbo and Tanga, 2009). This suggests that the thermal inertia of asteroids is mainly controlled by the dusty nature of the asteroid surface rather than other physical parameters associated to the nature of the material itself. This especially concerns thermal conductivity as thermal inertia only varies as the square root of the conductivity. Since (16) Psyche is a large main-belt asteroid, its surface should be also covered by such a thick and thermally insulating dust regolith, which would imply a low thermal inertia. Therefore, the high thermal inertia value we measured strongly suggests a significant difference in terms of composition, so that it would sufficiently increase the thermal conductivity of its surface and then its thermal inertia. This may also explain the potentially high thermal inertia (5–250 J m^{-2} $s^{-0.5}$ K^{-1}) measured for the large M-type Asteroid (22) Kalliope (Marchis et al., 2012). As stated in the introduction, metal is an excellent thermal conductor, potentially leading to an enhanced thermal inertia. In this context, Opeil et al. (2010) measured the thermal conductivity of a sample of meteorites including two ordinary chondrites, one enstatite chondrite, two carbonaceous chondrites and one iron meteorite. They showed that the thermal conductivity, at low temperatures (5–300 K), of iron meteorites is much higher, by about one order of magnitude, than the one of stony meteorites, especially the ordinary and carbonaceous chondrites. Interestingly, one order of magnitude difference in thermal conductivity corresponds to a factor 3–4 in thermal inertia, which is roughly the discrepancy between our thermal inertia measurement for (16) Psyche, around 120 J m^{-2} $s^{-0.5}$ K^{-1}, and the average thermal inertia of other large main-belt asteroids, around 30 J m^{-2} $s^{-0.5}$ K^{-1}. As a consequence, a metallic surface composition appears as a realistic explanation for the high thermal inertia we measured on the surface of (16) Psyche. Our results thus constitute a new evidence of the metal-rich composition of (16) Psyche, and confirm the previous radar studies on this object (e.g., Shepard et al., 2010).

We show in Fig. 5 all the existing thermal inertia measurements of main-belt asteroids larger than 100 km in diameter, including our measurement for (16) Psyche. We can see that the two M-type asteroids of the list, (16) Psyche and potentially (22) Kalliope, somehow sticks out from the thermal inertia range of large MBAs. This difference is even noticeable with P-type asteroids, which show thermal inertia values comparable to the one of C-complex and S-complex asteroids. This is in agreement with the expectation that P-type asteroids have surface materials rich in carbon and/or organics (Vilas et al., 1985; Hiroi et al., 2004), which are less thermally conductive. Fig. 5 thus illustrates how the relation between size and thermal inertia, highlighted for instance in Delbo and Tanga (2009), can be modified when asteroids with similar sizes but different compositions, especially metallic, are considered.

6. Summary

We have obtained the first successful interferometric observations of the M-type Asteroid (16) Psyche using the MIDI instrument and the 16 m-long baseline E0–G0 of the VLTI.

Following the work of Matter et al. (2011), we applied our thermophysical model (TPM) to the MIDI observations of (16) Psyche to derive its size and the thermal properties of its surface. Using the convex shape model of Kaasalainen et al. (2002), our TPM results indicate that Psyche has a volume equivalent diameter between 238 ± 24 and 247 ± 25 km, depending on the assumed surface roughness.

Our analysis also showed that a low macroscopic surface roughness is clearly favored by our interferometric observations, and that 'high roughness' models are discarded. With such a constraint on the macroscopic roughness, the TPM results indicate a high thermal inertia for (16) Psyche, of 133 J m^{-2} $s^{-0.5}$ K^{-1} ('no roughness') or 114 J m^{-2} $s^{-0.5}$ K^{-1} ('low roughness'), with a total uncertainty estimated at 40 J m^{-2} $s^{-0.5}$ K^{-1}. It is one of the highest thermal inertia values ever measured for a 200 km-class asteroid. This is in clear contradiction with previous results indicating that the surface of asteroids with sizes larger than 100 km have a low thermal inertia. As metal is an excellent thermal conductor, we expect this high thermal inertia to be another evidence of the metallic composition of (16) Psyche, as previously inferred from radar studies. This reinforces the hypothesis of (16) Psyche as originated from the fragmentation of the iron core of a differentiated parent body or more likely, considering its size, from the collision and aggregation of several objects, with at least one of them being purely metallic.

Acknowledgments

We would like to thank the referees for their comments and suggestions that helped to improve significantly this manuscript. We would also like to thank the staff and the Science Archive Operation of the European Southern Observatory (ESO) for their support in the data acquisition. We acknowledge support from the Faculty of the European Space Astronomy Centre (ESAC) for A. Matter's visit. The development of the asteroid thermophysical model used in this work was partially supported by the Project 11-BS56–008 (Shocks) of the Agence National de la Recherche (ANR). This research used the Miriade VO tool (Berthier et al., 2008) developed at IMCCE.

References

Bell, J.F., Davis, D.R., Hartmann, W.K., Gaffey, M.J., 1989. Asteroids – The big picture. In: Binzel, R.P., Gehrels, T., Matthews, M.S. (Eds.), University of Arizona Press, Asteroids II, pp. 921–945.

Berthier, J. et al., 2008. A service of position and physical ephemerides computation dedicated to the small bodies of the Solar System. LPI Contrib. 1405, 8374.

Bottke, W.F., Durda, D.D., Nesvorný, D., Jedicke, R., Morbidelli, A., Vokrouhlický, D., Levison, H.F., 2005. Linking the collisional history of the main asteroid belt to its dynamical excitation and depletion. Icarus 179, 63–94.

Bottke, W.F., Nesvorný, D., Grimm, R.E., Morbidelli, A., O'Brien, D.P., 2006. Iron meteorites as remnants of planetesimals formed in the terrestrial planet region. Nature 439, 821–824.

Bus, S.J., Binzel, R.P., 2002. Phase II of the small main-belt asteroid spectroscopic survey: A feature-based taxonomy. Icarus 158, 146–177.

Carry, B., 2009. Etude des propriétés physiques des astéroides par imagerie à haute résolution angulaire. Ph.D. Thesis, Université Paris 7 – Observatoire de Paris/LESIA.

Carry, B., 2012. Density of asteroids. Planet and Space Sci. 73, 98–118.

Cellino, A., Diolaiti, E., Ragazzoni, R., Hestroffer, D., Tanga, P., Ghedina, A., 2003. Speckle interferometry observations of asteroids at TNG. Icarus 162, 278–284.

Chesneau, O., 2007. MIDI: Obtaining and analysing interferometric data in the mid-infrared. New Astron. Rev. 51, 666–681.

Cloutis, E.A., Gaffey, M.J., Smith, D.G.W., Lambert, R.S.J., 1990. Metal silicate mixtures: Spectral properties and applications to asteroid taxonomy. J. Geophys. Res. 95, 8323–8338.

Cohen, M., Walker, R.G., Carter, B., Hammersley, P., Kidger, M., Noguchi, K., 1999. Spectral irradiance calibration in the infrared. X. A self-consistent radiometric all-sky network of absolutely calibrated stellar spectra. Astron. J. 117, 1864–1889.

Delbo, M., Tanga, P., 2009. Thermal inertia of main belt asteroids smaller than 100 km from IRAS data. Planet. Space Sci. 57, 259–265.

Delbo, M., Dell'Oro, A., Harris, A.W., Mottola, S., Mueller, M., 2007. Thermal inertia of near-Earth asteroids and implications for the magnitude of the Yarkovsky effect. Icarus 190, 236–249.

Delbo, M., Ligori, S., Matter, A., Cellino, A., Berthier, J., 2009. First VLTI–MIDI direct determinations of asteroid sizes. Astrophys. J. 694, 1228–1236.

DeMeo, F.E., Binzel, R.P., Slivan, S.M., Bus, S.J., 2009. An extension of the Bus asteroid taxonomy into the near-infrared. Icarus 202, 160–180.

Descamps, P., Marchis, F., Pollock, J., Berthier, J., Vachier, F., Birlan, M., Kaasalainen, M., Harris, A.W., Wong, M.H., Romanishin, W.J., Cooper, E.M., Kettner, K.A., Wiggins, P., Kryszczynska, A., Polinska, M., Coliac, J.-F., Devyatkin, A.,

Verestchagina, Gorshanov, D., . New determination of the size and bulk density of the binary Asteroid 22 Kalliope from observations of mutual eclipses. Icarus 196, 578–600.
Descamps, P., Marchis, F., Berthier, J., Emery, J.P., Duchêne, G., de Pater, I., Wong, M.H., Lim, L., Hammel, H.B., Vachier, F., Wiggins, P., Teng-Chuen-Yu, J.-P., Peyrot, A., Pollock, J., Assafin, M., Vieira-Martins, R., Camargo, J.I.B., Braga-Ribas, F., Macomber, B., 2011. Triplicity and physical characteristics of Asteroid (216) Kleopatra. Icarus 211, 1022–1033.
Drummond, J.D., Christou, J., 2006. Sizing up asteroids at lick observatory with adaptive optics. In: AAS/Division for Planetary Sciences Meeting, vol. 38. Bulletin of the American Astronomical Society. Abstracts 1304.
Drummond, J., Christou, J., 2008. Triaxial ellipsoid dimensions and rotational poles of seven asteroids from Lick Observatory adaptive optics images, and of Ceres. Icarus 197, 480–496.
Durech, J., Sidorin, V., Kaasalainen, M., 2010. DAMIT: A database of asteroid models. Astron. Astrophys. 513, A46.
Durech, J., Kaasalainen, M., Herald, D., Dunham, D., Timerson, B., Hanuš, J., Frappa, E., Talbot, J., Hayamizu, T., Warner, B.D., Pilcher, F., Galád, A., 2011. Combining asteroid models derived by lightcurve inversion with asteroidal occultation silhouettes. Icarus 214, 652–670.
Emery, J.P., Cruikshank, D.P., van Cleve, J., 2006. Thermal emission spectroscopy (5.2–38 μm) of three Trojan asteroids with the Spitzer Space Telescope: Detection of fine-grained silicates. Icarus 182, 496–512. http://dx.doi.org/10.1016/j.icarus.2006.01.011.
Fornasier, S., Clark, B.E., Dotto, E., Migliorini, A., Ockert-Bell, M., Barucci, M.A., 2010. Spectroscopic survey of M-type asteroids. Icarus 210, 655–673.
Hanus, J., Marchis, F., Durech, J., 2012. Asteroid sizes determined by combining shape models and keck adaptive optics images. In: AAS/Division for Planetary Sciences Meeting, vol. 44. Abstracts 302.08.
Hapke, B., 1984. Bidirectional reflectance spectroscopy. III – Correction for macroscopic roughness. Icarus 59, 41–59.
Hardersen, P.S., Gaffey, M.J., Abell, P.A., 2005. Near-IR spectral evidence for the presence of iron-poor orthopyroxenes on the surfaces of six M-type asteroids. Icarus 175, 141–158.
Hiroi, T. et al., 2004. What are the P-type asteroids made of? In: Mackwell, S., Stansbery, E. (Eds.), Lunar and Planetary Institute Science Conference Abstracts, vol. 35. Lunar and Planetary Inst. Technical Report, 1616.
Jaffe, W.J., 2004. Coherent fringe tracking and visibility estimation for MIDI. In: Traub, W.A. (Ed.), Society of Photo-Optical Instrumentation Engineers (SPIE) Conference Series, vol. 5491, p. 715.
Jakosky, B.M., 1986. On the thermal properties of martian fines. Icarus 66, 117–124.
Jakosky, B.M., Finiol, G.W., Henderson, B.G., 1990. Directional variations in thermal emission from geologic surfaces. Geophys. Res. Lett. 17, 985–988.
Kaasalainen, M., Torppa, J., 2001. Optimization methods for asteroid lightcurve inversion. I. Shape determination. Icarus 153, 24–36.
Kaasalainen, M., Torppa, J., Piironen, J., 2002. Models of twenty asteroids from photometric data. Icarus 159, 369–395.
Kuzmanoski, M., Kovačević, A., 2002. Motion of the Asteroid (13206) 1997GC22 and the mass of (16) Psyche. Astron. Astrophys. 395, L17–L19.
Lamy, P.L., Groussin, O., Fornasier, S., Jorda, L., Kaasalainen, M., Barucci, M.A., 2010. Thermal properties of Asteroid 21 Lutetia from Spitzer Space Telescope observations. Astron. Astrophys. 516, A74.
Lebofsky, L.A., Sykes, M.V., Tedesco, E.F., Veeder, G.J., Matson, D.L., Brown, R.H., Gradie, J.C., Feierberg, M.A., Rudy, R.J., 1986. A refined 'standard' thermal model for asteroids based on observations of 1 Ceres and 2 Pallas. Icarus 68, 239–251.
Leinert, C. et al., 2004. Mid-infrared sizes of circumstellar disks around Herbig Ae/Be stars measured with MIDI on the VLTI. Astron. Astrophys. 423, 537–548.
Leyrat, C., Barucci, A., Mueller, T., O'Rourke, L., Valtchanov, I., Fornasier, S., 2012. Thermal properties of (4) Vesta derived from Herschel measurements. Astron. Astrophys. 539, A154.
Lupishko, D.F., 2006. On the bulk density of the M-type Asteroid 16 Psyche. Solar Syst. Res. 40, 214–218. http://dx.doi.org/10.1134/S0038094606030051.
Marchis, F., Enriquez, J.E., Emery, J.P., Mueller, M., Baek, M., Pollock, J., Assafin, M., Vieira Martins, R., Berthier, J., Vachier, F., Cruikshank, D.P., Lim, L.F., Reichart, D.E., Ivarsen, K.M., Haislip, J.B., LaCluyze, A.P., 2012. Multiple asteroid systems: Dimensions and thermal properties from Spitzer Space Telescope and ground-based observations. Icarus 221, 1130–1161.
Matter, A., Delbo, M., Ligori, S., Crouzet, N., Tanga, P., 2011. Determination of physical properties of the Asteroid (41) Daphne from interferometric observations in the thermal infrared. Icarus 215, 47–56.
Mueller, M., 2007. Surface Properties of Asteroids from Mid-infrared Observations and Thermophysical Modeling. Ph.D. Thesis, Freie Universitaet, Berlin, 2007.
Mueller, T.G., Lagerros, J.S.V., 1998. Asteroids as far-infrared photometric standards for ISOPHOT. Astron. Astrophys. 338, 340–352.
Mueller, M., Marchis, F., Emery, J.P., Harris, A.W., Mottola, S., Hestroffer, D., Berthier, J., di Martino, M., 2010. Eclipsing binary Trojan asteroid Patroclus: Thermal inertia from Spitzer observations. Icarus 205, 505–515.
Müller, T.G., Blommaert, J.A.D.L., 2004. 65 Cybele in the thermal infrared: Multiple observations and thermophysical analysis. Astron. Astrophys. 418, 347–356.
Opeil, C.P., Consolmagno, G.J., Britt, D.T., 2010. The thermal conductivity of meteorites: New measurements and analysis. Icarus 208, 449–454.
O'Rourke, L. et al., 2012. Thermal and shape properties of Asteroid (21) Lutetia from Herschel observations around the Rosetta flyby. Plan. and Space Sci. 66, 192–199.
Ostro, S.J., Campbell, D.B., Shapiro, I.I., 1985. Mainbelt asteroids – Dual-polarization radar observations. Science 229, 442–446.
Perrin, G., Leinert, C., Graser, U., Waters, L.B.F.M., Lopez, B., 2003. MIDI, the 10 μm interferometer of the VLT. In: Perrin, G., Malbet, F. (Eds.), EAS Publications Series, vol. 6, EDP sciences, p. 127.
Pravec, P., Harris, A.W., Kušnirák, P., Galád, A., Hornoch, K., 2012. Absolute magnitudes of asteroids and a revision of asteroid albedo estimates from WISE thermal observations. Icarus 221, 365–387.
Rivkin, A.S., Howell, E.S., Britt, D.T., Lebofsky, L.A., Nolan, M.C., Branston, D.D., 1995. Three-micron spectrometric survey of M- and E-class asteroids. Icarus 117, 90–100.
Rivkin, A.S., Howell, E.S., Lebofsky, L.A., Clark, B.E., Britt, D.T., 2000. The nature of M-class asteroids from 3-micron observations. Icarus 145, 351–368.
Shepard, M.K., Clark, B.E., Nolan, M.C., Howell, E.S., Magri, C., Giorgini, J.D., Benner, L.A.M., Ostro, S.J., Harris, A.W., Warner, B., Pray, D., Pravec, P., Fauerbach, M., Bennett, T., Klotz, A., Behrend, R., Correia, H., Coloma, J., Casulli, S., Rivkin, A., 2008. A radar survey of M- and X-class asteroids. Icarus 195, 184–205.
Shepard, M.K., Clark, B.E., Ockert-Bell, M., Nolan, M.C., Howell, E.S., Magri, C., Giorgini, J.D., Benner, L.A.M., Ostro, S.J., Harris, A.W., Warner, B.D., Stephens, R.D., Mueller, M., 2010. A radar survey of M- and X-class asteroids II. Summary and synthesis. Icarus 208, 221–237.
Sih, S.S., Barlow, J.W., 2004. The prediction of the emissivity and thermal conductivity of powder beds. Particulate Sci. Technol. 22 (4), 427–440. http://dx.doi.org/10.1080/02726350490501682.
Tedesco, E.F., Noah, P.V., Noah, M., Price, S.D., 2002. The supplemental IRAS minor planet survey. Astron. J. 123, 1056–1085.
Tholen, D.J., 1984. Asteroid Taxonomy from Cluster Analysis of Photometry. Ph.D. Thesis, Arizona Univ., Tucson.
Usui, F. et al., 2011. Asteroid catalog using Akari: AKARI/IRC mid-infrared asteroid survey. Publ. Astron. Soc. Japan 63, 1117–1138.
Verhoelst, T., 2005. Evolved stars: A combined view VROM interferometry and spectroscopy. Ph.D. Thesis, Institute of Astronomy, K.U. Leuven, Belgium.
Veverka, J. et al., 2001a. The landing of the NEAR-Shoemaker spacecraft on Asteroid 433 Eros. Nature 413, 390–393.
Veverka, J. et al., 2001b. Imaging of small-scale features on 433 Eros from NEAR: Evidence for a complex regolith. Science 292, 484–488.
Viateau, B., 2000. Mass and density of Asteroids (16) Psyche and (121) Hermione. Astron. Astrophys. 354, 725–731.
Vilas, F., Smith, B.A., 1985. Reflectance spectrophotometry (about 0.5–1.0 micron) of outer-belt asteroids – Implications for primitive, organic Solar System material. Icarus 64, 503–516.
Yano, H. et al., 2006. Touchdown of the Hayabusa Spacecraft at the Muses Sea on Itokawa. Science 312, 1350–1353.